Available online at www.sciencedirect.com
SCIENCE DIRECT®
Catalysis Today 93–95 (2004) 529–534
CATALYSIS TODAY
www.elsevier.com/locate/cattod

Hydrothermally stable MCM-41 analogue with extensive embedded voids

Junlin Zheng [a], Shangru Zhai [a], Ye Zhang [a], Dong Wu [a], Yuhan Sun [a,*], Yongxia Yang [b], Lei Chen [b], Feng Deng [b]

[a] *State Key Laboratory of Coal Conversion, Institute of Coal Chemistry, Chinese Academy of Sciences, Taiyuan 030001, PR China*
[b] *State Key Laboratory of Magnetic Resonance and Atomic Molecular Physics, Wuhan Institute of Physics and Mathematics, Chinese Academy of Sciences, Wuhan 430071, PR China*

Abstract

Hydrothermally stable aluminosilicate MCM-41 analogue with extensive embedded voids was prepared via the controlled coassembly of protozeolitic nanoclusters and soluble silicates in alkaline media. XRD, N_2 sorption results showed that the sample had highly ordered hexagonal mesostructures typical of MCM-41, but the hydrothermal stability was largely improved compared to normal MCM-41 merely from sodium silicates and sodium aluminates. Furthermore, the MCM-41 analogue exhibited tubular morphology in typical SEM micrograph, and embedded voids were extensively distributed in the tubule walls based on TEM observation and N_2 sorption analysis. As a result, the unidimensional nanochannels were interconnected into three-dimensional networks by these embedded voids. NMR results indicated that the MCM-41 analogue had higher cross-linking degree compared to normal MCM-41, which led to the greatly improved hydrothermal stability. This MCM-41 analogue with good hydrothermal stability and increased interchannel accessibility is a potential candidate as catalysts and catalyst supports.

Keywords: MCM-41; Protozeolitic nanoclusters; Hydrothermal stability; Voids

1. Introduction

Hexagonally ordered MCM-41 is one of the most important members in mesoporous aluminosilicates family [1,2]. Because of its convenient synthesis procedure, adjustable hexagonal mesopores, and facile silica sources, the synthesis and applications of MCM-41 have been intensively investigated in the past decade [3]. However, there are two main obstacles in applying MCM-41 as catalysts or catalyst supports. The long and unidimensional nanochannels of MCM-41 have disadvantage in the diffusion and transport of reactants and products, which limits practical applications in catalysis and separation [4]. The other concern is the poor hydrothermal stability, i.e., the mesostructures are inclined to degrade in wet conditions at elevated temperature, which is widely attributed to the thinness and incomplete cross-linking of the pore walls. This would make its long-term use in a reaction stream and regeneration doubtful if water were involved in the system.

Recently, many methods have been developed to improve the hydrothermal stability of MCM-41, such as repeated pH adjustment [5], salt effects [6] and post-synthesis restructure [7]. However, the most significant improvement in the hydrothermal stability of aluminosilicate mesostructures resulted from the use of protozeolitic nanoclusters as precursors for direct assembly [8–10]. Xiao and co-workers [8] and Pinnavaia and co-workers [9] have developed the method to synthesize hydrothermally stable mesoporous aluminosilicates of MCM-41 type using protozeolitic nanoclusters as building units in alkaline media. The excellent hydrothermal stability was greatly attributed to the successful introduction of zeolite subunits into the mesostructured framework walls upon assembling these nanoclusters into mesostructured materials and consequent increased framework cross-linking degree [10].

It is highly desirable to not only improve the hydrothermal stability but also interconnect the unidimensional nanochannels of MCM-41 for practical applications in catalysis.

* Corresponding author. Tel.: +86 351 406 3121; fax: +86 351 404 1153.
E-mail addresses: yhsun@sxicc.ac.cn, zjl604@sxicc.ac.cn (Y. Sun).

0920-5861/$ – see front matter © 2004 Elsevier B.V. All rights reserved.
doi:10.1016/j.cattod.2004.06.003

Herein, we present a method to prepare hydrothermally stable MCM-41 analogue with extensive embedded voids via the controlled coassembly of protozeolitic nanoclusters and soluble silicates. Aluminosilicate precursor solution comprising Beta protozeolitic nanoclusters were prepared under the direction of short chain organic amine. A neutralization process of the strongly alkaline system was adopted to initiate the self-assembly of surfactant–silicate and silica condensation separately.

2. Experimental

2.1. Materials

Typical synthesis procedure can be referred to the reported literature [11]: (1) Aluminosilicate precursor solution containing abundant protozeolitic nanoclusters was prepared by the reaction of tetraethylammonium hydroxide (TEAOH), sodium aluminates, sodium hydroxide, and fumed silica in water at 140 °C for 4 h, and the $Al_2O_3/SiO_2/Na_2O/TEAOH/H_2O$ molar ratio is 1.0/60/2.5/22/800. (2) A certain amount of sodium silicates (SiO_2/Na_2O is 1.03) and sodium aluminates ($SiO_2/Al_2O_3 = 60$) were dissolved in the cetyltrimethylammonium bromide (CTAB) template solution. The precursor solution was also added into the mixture to get an opaque white suspension, when the pH value was above ca. 13. The quantity of SiO_2 from precursor solution was equal to that from sodium silicates. Molar ratio of the final gel was: $Al_2O_3/SiO_2/CTAB/H_2O = 1.0/60/17/(3000–4800)$. (3) After stirring for 10 min, the pH value was adjusted to 10 through adding proper amount of H_2SO_4 (2 M) into the mixture. The final mixture was hydrothermally treated in an autoclave at 110 °C for 48 h. After filtered, washed and dried, the precipitates were then calcined at 550 °C for 6 h to remove the organic templates. Normal MCM-41 tubules were synthesized adopting a delayed neutralization process of 30 min according to the literature [12–14], and the molar ratio of $Al_2O_3/SiO_2/CTAB/H_2O$ was 1/60/28.8/(3000–4800) in the starting system. Hydrothermal stability was evaluated by aging the samples in boiling water for 150 h.

2.2. Characterization

The X-ray diffraction (XRD) patterns were recorded using a Shimadzu XD-3A X-ray powder diffractometer, which employed Ni-filtered Cu Kα radiation and were operated at 40 kV and 30 mA. The N_2 adsorption and desorption isotherms at 77 K were measured using a Micromeritics Tristar 3000 system. The adsorption and desorption pore distribution plots were analyzed from adsorption and desorption branches of the isotherms, respectively, by the Barrett–Joyner–Halenda (BJH) model with Halsey equation for multiplayer thickness. The first pore in desorption pore distribution plot was adopted as approximate pore size. Repeat distance (a_o) was calculated by X-ray diffraction data with the equation $a_o = 2d_{100}/3^{0.5}$. The wall thickness was determined by the difference between the repeat distance (a_o) and approximate pore size. Scanning electron microscopy (SEM) was performed on Philips XL30FEG apparatus. Transmission electron microscopy (TEM) was recorded on a Philips CM200FEG instrument with acceleration voltage of 200 kV. ^{29}Si MAS NMR spectra were recorded on a Bruker MSL-400 spectrometer.

3. Results and discussion

3.1. XRD and N_2 sorption results

Fig. 1 shows the XRD patterns of as-made sample (A) and normal MCM-41 (B) before (a) and after (b) treatment in boiling water for 150 h. The sample has three sharp diffraction peaks that can be attributed to (1 0 0), (1 1 0), and (2 0 0) reflections, and the d_{100} value is 4.15 nm. The highly mesoscopic degree is preserved after 150 h treatment in boiling water although the intensity of (1 0 0) peak decreases slightly. Normal MCM-41 prepared under the direction of CTAB template using sodium silicates as silica source and sodium aluminates as aluminum source also shows high-quality mesostructures evidenced by the presence of (1 0 0), (1 1 0) and (2 0 0) diffraction peaks, and the d_{100} value is 3.81 nm. But these peaks disappear completely after 150 h age in boiling water. So it is feasible to produce mesoporous aluminosilicates with well-ordered hexagonal structure of MCM-41 type through controlled coassembly of protozeolitic nanoclusters and soluble silica species, and the obtained material possesses good hydrothermal stability.

The N_2 adsorption/desorption isotherms of the sample are shown in Fig. 2. For the sample before aging, a steep increase occurs in the type IV isotherm curve at the relative pressure of $0.3 < p/p_o < 0.4$, which can be attributed to the presence of highly ordered mesostructures. After aged (b),

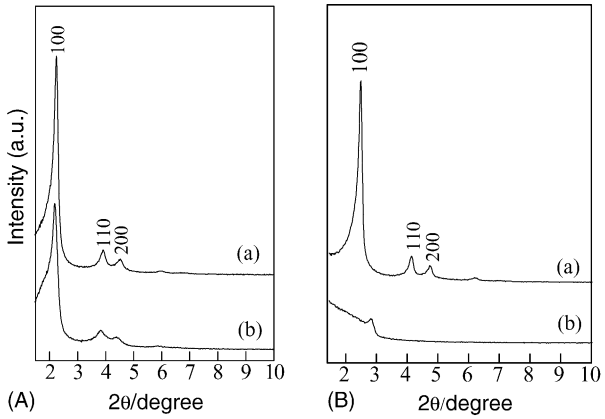

Fig. 1. The XRD patterns of resultant MCM-41 analogue (A) and normal MCM-41 (B) before (a) and after (b) aged in boiling water for 150 h.

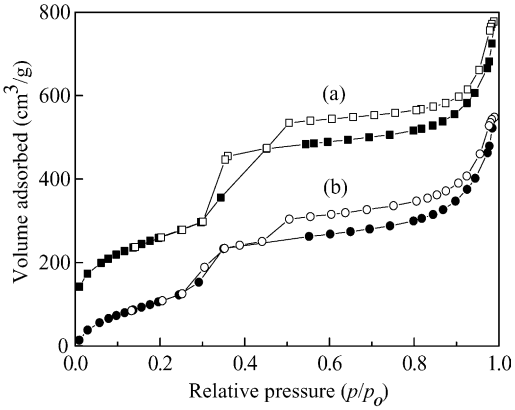

Fig. 2. N_2 adsorption (solid)/desorption (hollow) isotherms of the MCM-41 analogue before (a) and after (b) aged in boiling water for 150 h.

the highly regular mesostructures are preserved. Besides the inflection characteristic of capillary condensation process in regular mesopores, additional uncommon type-H4 hysteresis loops above $p/p_o = 0.5$ can be observed in the N_2 sorption isotherms of the sample. Although the volume adsorbed in the adsorption and desorption branch shows a comparable trend at higher p/p_o values ($p/p_o = 0.5$), a quite different phenomenon appears around $p/p_o = 0.45$. The adsorption branch shows a progressive increase in the volume adsorbed corresponding to a broad distribution of textural mesoporosity. In contrast, the desorption branch shows a pronounced step around $p/p_o = 0.45$ resulting in the closure of the hysteresis loop. It can also be observed that the ascending of adsorption isotherm is slightly faster than that of desorption one above $p/p_o = 0.5$. Pore size distribution plots are calculated using the BJH algorithm employing adsorption (a) and desorption (b) branches, respectively (Fig. 3). The plot from adsorption data shows a mesopore at diameter of 3.20 nm, while another additional 3.70 nm mesopore following the mesopore at the mean diameter of 2.67 nm is present in the plot from desorption isotherm. The clear differences in desorption and adsorption pore size distribution plots indicate

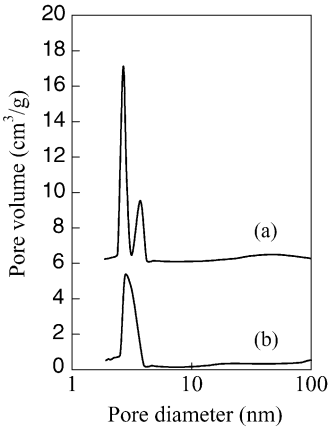

Fig. 3. BJH desorption (a) and adsorption (b) pore size distribution plots of the MCM-41 analogue.

Fig. 4. SEM micrograph of the MCM-41 analogue.

the non-physical nature of the 3.70 nm mesopore. Hysteresis loop is usually attributed to the thermodynamic or network effects or the combination of these two effects. The particular hysteresis loops in N_2 sorption isotherms hint unusual structural character and deserve further investigation. In combination with TEM micrograph, the unusual hysteresis loops and pore size distribution plots will be systematically analyzed to unveil the particular structural character in the latter parts.

3.2. Tubular morphology

SEM is performed to examine the morphology of the MCM-41 analogue. It illustrates that the MCM-41 analogue has tubular morphology (see Fig. 4) [11], which is similar to that of normal aluminosilicate MCM-41 tubules merely from sodium silicates and sodium aluminates reported previously [12–14]. Based on systematic SEM observations, it is estimated that about 90% of the solid materials show regular tubular morphology with mean diameter of 0.30 μm and average length of 2.0 μm.

Previous researchers have investigated this tubular morphology intensively, and detailed descriptions and discussions can be found therein [12–14]. In these studies, a special “delayed neutralization process” based on the consideration of temporal separation of self-assembly of surfactant–silicate and silica condensation was employed to synthesize hierarchical tubules-within-tubule (TWT) MCM-41. The addition of sodium silicates made the gel system strongly alkaline. In the beginning, the aluminosilicate–surfactant system was close to the lamellar-hexagonal phase boundary under high pH value, and a little acidification resulted in a mixed lamellar-hexagonal phase in which layers of hexagonally arranged rod micelles were separated by bilayers of surfactants and water. Because the membrane layers were intrinsically anisotropic, further acidification leading to the condensation of silicates and charge imbalance on the mem-

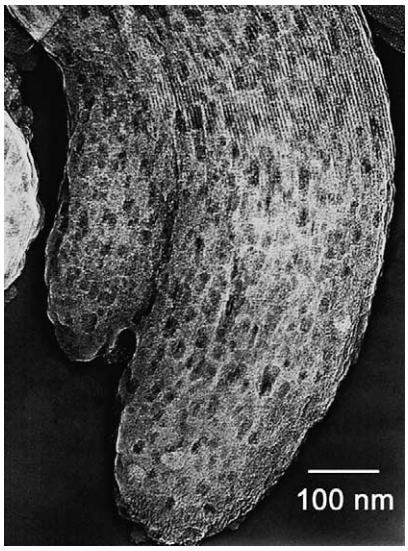

Fig. 5. TEM micrograph of the mesostructured tubule.

brane surface favored the curvature of the membrane along the transrod direction. Thus, tubular morphology evolved. The probable formation mechanism of the microtubules proposed by Lin and Mou et al. holds true here despite the extra introduction of protozeolitic nanoclusters in the present experiments. In our experiments, it is not necessary to obey the strongly recommended 30 min slow neutralization process. Tubular mesoporous aluminosilicates can be fabricated conveniently in a fast acidification process. Comparing with the former system, the introduction of protozeolitic nanoclusters is the exclusively possible reason for the facilitation of synthesis procedure. The densely distributed protozeolitic nanoclusters probably aggravated the charge imbalance on the bilayer membrane surface, and thus the force driving the curvature of the membrane increased. Thus the microtubules are fabricated conveniently via the coassembly of protozeolitic nanoclusters and soluble silica species in this rapid acidification process.

3.3. Extensive embedded voids

Fig. 5 shows the TEM micrograph of a single tubule of the current MCM-41 analogue. XRD characterizations have substantiated the presence of well-ordered hexagonal mesostructures. The equidistant parallel lines along the axes outside the tubule wall correspond to the (1 1 0) spaces of hexagonal mesostructure. Furthermore, the TEM micrograph provides more important structural characters. The darkness of the tubules is not uniform. The gray parts are concrete mesostructured frameworks. The dark spots that distribute extensively in the tubule walls can be ascribed to the presence of many submicron-sized structural defect voids, which are irregular shaped and the size distributes between 5 and 30 nm.

The presence of extensive embedded voids in the mesostructured framework can effectively explain the uncommon hysteresis loops and the clear difference in pore size distribution plots. The defect voids imbedded in the tubule walls are surrounded by well-aligned nanochannels of the MCM-41 analogue. In the adsorption isotherm, the single steep rise in volume reflects the size of nanochannels in capillary condensation. With the increase of pressure above $p/p_o = 0.5$, N_2 were progressively adsorbed into the defect voids through the surrounding mesopores. In the desorption process of adsorbed N_2, since the mesopores surrounding the internal voids are still filled with condensed adsorbate, the internal voids cannot be emptied at the relative pressure corresponding to the capillary evaporation of them. After the mesopores are emptied, the driving force for the evaporation of N_2 in the internal voids is strong enough that a lot of cooperative evaporation happens at the same pressure. N_2 rushes out altogether to form an additional inflection in desorption branch, which also is the cause of the artificial 3.70 nm pore in desorption branch derived pore size distribution plot [15,16]. Previous literature has briefly discussed the non-physical nature of the artificial 3.70 nm mesopore [17]. Desorption of adsorbed N_2 only happens in the textural pores above $p/p_o = 0.5$, so the ascending of adsorption isotherm is slightly faster than that of desorption one.

Tubular morphology is often associated with more defects and thus larger hysteresis behavior. The bending and closing-up process in a membrane-to-tubule transformation would unavoidably create some stress, and thus packing defects, between the cylindrical micelles. When further silica condensation happened, the extra interlayer water was expulsed to form little puddles and many internal defect voids thus formed as the relic of water puddles [16]. The previous results showed that the formation of structural defects in the MCM-41 tubules depended mainly on the amount of incorporated aluminium. According to Loweinstein's rule, crystalline aluminosilicates such as zeolites generally avoid the formation of Al–O–Al moieties in their framework. The size of MCM-41 particle is reduced by the incorporation of Al into the silica framework. This factor makes the nanochannel of aluminosilicate MCM-41 shorter than that of silica MCM-41, and then the shorter nanorods in the synthesis media then restructure into a more defective framework. In our experiments, MCM-41 analogue with extensive embedded voids cannot be fabricated merely from protozeolitic nanoclusters. Perhaps the Al elements fixed in protozeolitic nanoclusters cannot act on the formation of defect voids independently. When sodium silicates and sodium aluminates are added in the system, soluble Al species from sodium aluminates lead to the formation of extensive embedded voids in this coassembly approach. Accompanying the addition of aluminosilicate precursor solution, sodium silicates and sodium aluminates serving as another part of precursors pave the way for morphology and structure tailoring of this material.

The existence of extensive embedded voids increases the porosity and can act as reservoirs connecting neigh-

boring unidimensional nanochannels. So the original one-dimensional network becomes effectively inter-connected, and the diffusion and transport of larger molecules become easier in such void systems and the mixing of molecules across the channels is easier. The effectively inter-connected network will greatly benefit the practical application of this MCM-41 type mesoporous aluminosilicates.

3.4. Self-assembly process

The analysis of hydrolysis and condensation behaviors of protozeolitic nanoclusters and soluble silica species in this route would be helpful to unveil the coassembly process. Aluminosilicate precursor solution and sodium silicates supplied different structural building units in the construction of mesostructures. After sodium silicates and precursor solution were added into the CTAB solution, most of the soluble silica species from sodium silicates were deprotonated and in the form of oligomers above ca. pH 12 [18]; the protozeolitic nanoclusters reserved their original forms in precursor solution, and the pK_a value was lower than that of the oligomers. For monomeric $Si(OH)_4$, the pK_a value was about 9.8 at room temperature, but it shifted to 6.5 gradually as siloxane condensation progresses [19]. Larger particles with higher condensation degree had increasing acidity (lower pK_a value), which were well charged in alkaline media and competitive in exchanging the micellar counterion Br^- to initiate the self-assembly process ($S^+Br^- + I^- \rightarrow S^+I^- + Br^-$). In the neutralization process, the energetically advantageous nanoclusters interacted with CTAB template micella to initiate the self-assembly process primarily. The mesostructures were built up by condensation processes, where the anchored nanoclusters acted as nucleation points. According to the Ostwald ripening mechanism, those poorly condensed oligomers from sodium silicates tended to dissolve into $Si(OH)_4$ monomers and deposited on the surface of highly condensed protozeolitic nanoclusters to enrich the mesostructures in the neutralization process. The deposited $Si(OH)_4$ monomers probably made the membrane layers relatively flexible to curl into tubules at the same time. Thus, protozeolitic nanoclusters entered the framework of resultant mesostructures. Furthermore, the protozeolitic nanoclusters serving as nucleating centers probably promoted the condensation of non-structure silica and aluminum species from sodium silicates and sodium aluminates on their surfaces, which was different from the loose polymerization behavior of normal MCM-41 merely from sodium silicates and sodium aluminates.

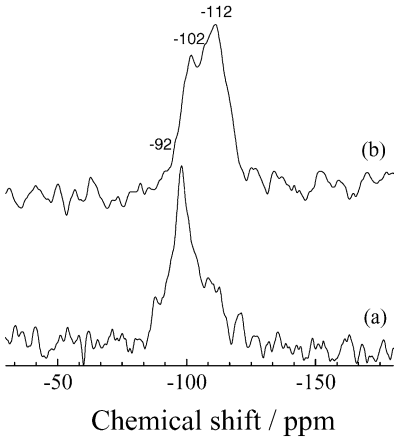

Fig. 6. ^{29}Si MAS NMR spectra of as-synthesized normal MCM-41 (a) and MCM-41 analogue (b).

3.5. Hydrothermal stability

Calculated from XRD and N_2 sorption results, the textural properties of so-produced materials and normal MCM-41 are displayed in Table 1. The BET surface area of the sample decreases from 947 to 750 $m^2\,g^{-1}$ after 150 h aged in boiling water, and the pore volume decreases from 1.03 to 0.87 $cm^3\,g^{-1}$. Most of the surface area and pore volume are maintained after 150 h aged in boiling water. In contrast, the BET surface area of normal MCM-41 decreases sharply from 1140 to 340 $m^2\,g^{-1}$ after aged. All of them reveal the superior hydrothermal stability to that of normal MCM-41.

The local structure of the silicate subunits comprising the framework walls and the degree of overall framework cross-linking are two dominating factors influencing the hydrothermal stability of a mesostructured aluminosilicate framework [20]. Fig. 6 is the ^{29}Si MAS NMR spectra of normal MCM-41 (a) and the MCM-41 analogue via coassembly route (b). The peak at 112 and 102 ppm can be indexed as Q_4 and Q_3, respectively. Q_4/Q_3 is an efficient factor indicating the overall cross-linking degree of the framework, that is, higher Q_4/Q_3 value reflects the higher cross-linking degree of mesostructured aluminosilicate framework. The Q_4/Q_3 value of the MCM-41 analogue is 2.5, while that of normal MCM-41 is only 1.0. So this MCM-41 analogue has higher cross-linking degree compared with normal MCM-41 through the extra introduction of protozeolitic nanoclusters.

Table 1
Textural properties of as-made sample and MCM-41 before and after treatment in boiling water for 150 h

Sample	Age time (h)	d_{100} (nm)	Pore diameter (nm)	Wall thickness (nm)	S_{BET} ($m^2\,g^{-1}$)	Pore volume ($cm^3\,g^{-1}$)
As-made sample	0	4.15	2.67	2.12	947	1.03
	150	4.14	2.68	2.10	750	0.87
MCM-41	0	3.81	2.63	1.77	1140	1.08
	150	–	–	–	340	0.65

In the reported literatures, protozeolitic nanoclusters could be directly assembled into hydrothermally stable hexagonal, wormlike, and foamlike framework structures under a variety of assembly conditions [8–10]. Coating of protozeolitic nanoclusters on the walls of pre-assembled frameworks also led to hydrothermally stable derivatives [21,22]. In present procedures, mesoporous aluminosilicates with hollow tubular morphology and hexagonal nanochannels were prepared via the controlled coassembly of protozeolitic nanoclusters, sodium silicates, and sodium aluminates. As the protozeolitic nanoclusters are assembled into the framework of the mesostructure in alkaline media, the zeolite-like connectivity of tetrahedral AlO_4 and SiO_4 units are deservedly reserved in the mesostructures, and they help to improve the framework cross-linking degree. So the protozeolitic nanoclusters entering the mesostructured framework as one part of precursors enhance the hydrothermal stability of the resultant mesoporous aluminosilicates, which can be regarded as active ingredient of hydrothermal stability.

The framework wall thickness of the as-synthesized MCM-41 analogue is 2.12 nm, which is 0.35 nm thicker than the 1.77 nm framework wall of normal MCM-41. The increased wall thickness can be attributed to the following reason. Protozeolitic nanoclusters in precursor solution have stronger rigidity and larger volume than that of the nonstructural aluminosilicate species from sodium silicates and sodium aluminates in the synthesis of normal MCM-41, so the framework walls get thicker to accommodate the nanoclusters [8]. The thicker wall assists the improvement of hydrothermal stability.

4. Conclusions

Hydrothermally stable mesoporous aluminosilicates with extensive embedded voids and hexagonal mesostructures were fabricated via the controlled coassembly of protozeolitic nanoclusters and soluble silicates. Protozeolitic nanoclusters improved the hydrothermal stability of the obtained mesoporous aluminosilicates. Sodium silicates donating soluble silica species made the assembly system strongly alkaline, then abundant embedded voids formed in the fabrication of mesostructured tubules. Thus the one-dimensional nanochannels were effectively inter-connected as a three-dimensional network for the presence of these voids. Combining the properties of more effective interchannel accessibility, high hydrothermal stability and large surface areas, this aluminosilicate MCM-41 analogue is particularly suitable for industrially important catalytic reactions such as dehydrogenation, hydrocracking and alkylation.

Acknowledgements

Financial supports from the National Key Basic Research Special Foundation (G2000048001) are gratefully acknowledged.

References

[1] C.T. Kresge, M.E. Leonowicz, W.J. Roth, J.C. Vartuli, J.S. Beck, Nature 359 (1992) 710.
[2] J.S. Beck, J.C. Vartuli, W.J. Roth, M.E. Leonowicz, C.T. Kresge, K.O. Schmitt, C.T.-W. Chu, D.H. Olson, E.W. Sheppard, S.B. McCullen, J.B. Higgins, J.L. Schlenker, J. Am. Chem. Soc. 114 (1992) 10834.
[3] A. Corma, Chem. Rev. 97 (1997) 2373.
[4] M. Rozwadowski, M. Lezanska, J. Wloch, K. Erdmann, R. Golembiewski, J. Kornatowski, Chem. Mater. 13 (2001) 1609.
[5] D. Das, C.M. Tsai, S. Cheng, Chem. Commun. (1999) 473.
[6] J.M. Kim, S. Jun, R. Ryoo, J. Phys. Chem. B 103 (1999) 6200.
[7] R. Mokaya, Adv. Mater. 22 (2000) 1681.
[8] Z.T. Zhang, Y. Han, F.-S. Xiao, S.L. Qiu, L. Zhu, R.W. Wang, Y. Yu, Z. Zhang, B.S. Zou, Y.Q. Wang, H.P. Sun, D.Y. Zhao, Y. Wei, J. Am. Chem. Soc. 123 (2001) 5014.
[9] Y. Liu, W.Z. Zhang, T.J. Pinnavaia, Angew. Chem. Int. Ed. 40 (2001) 1255.
[10] Y. Liu, T.J. Pinnavaia, J. Mater. Chem. 12 (2002) 3179.
[11] J.L. Zheng, Y. Zhang, Z.H. Li, W. Wei, D. Wu, Y.H. Sun, Chem. Phys. Lett. 376 (2003) 136.
[12] H.-P. Lin, C.-Y. Mou, Science 273 (1996) 765.
[13] H.-P. Lin, S. Cheng, C.-Y. Mou, Chem. Mater. 10 (1998) 581.
[14] H.-P. Lin, C.-Y. Mou, Acc. Chem. Res. 35 (2002) 927.
[15] S.-T. Wong, H.-P. Lin, S. Cheng, C.-Y. Mou, Appl. Catal. A: General 198 (2000) 103.
[16] H.-P. Lin, S.-T. Wong, C.-Y. Mou, C.-Y. Tang, J. Phys. Chem. B 104 (2000) 8967.
[17] J.C. Groen, L.A.A. Peffer, J. Pérez-Ramírez, Micropor. Mesopor. Mater. 51 (2002) 75.
[18] C.J. Brinker, G.W. Scherer, The Physics and Chemistry of Sol–Gel Processing, Academic Press, San Diego, 1990.
[19] R.K. Iler, The Chemistry of Silica: Solubility, Polymerization, Colloid and Surface Properties, and Biochemistry, Wiley, New York, 1979.
[20] R.P. Pauly, V. Petkov, Y. Liu, S.J. Billinge, T.J. Pinnavaia, J. Am. Chem. Soc. 124 (2002) 97.
[21] D. Trong On, S. Kaliaguine, Angew. Chem. Int. Ed. 41 (2002) 1036.
[22] D. Trong On, S. Kaliaguine, J. Am. Chem. Soc. 125 (2003) 618.